Journal of Engineering Science and Technology
Vol. 12, No. 6 (2017) 1640 - 1661

NUMERICAL INVESTIGATION OF THE COUPLED TURBULENT COMBUSTION-RADIATION IN AN AXISYMMETRIC NON-PREMIXED FLAME

BRAHIM ZITOUNI, RACHID MECHI, HABIB FARHAT*, RACHID SAID

Laboratory of Studies of Ionized and Reactive Media, Preparatory Institute of Studies in Engineering of Monastir, Ibn El-Jazzar Street 5019 Monastir, Tunisia
*Corresponding Author: habib.farhat@ipeim.rnu.tn

Abstract

A turbulent non-premixed methane-air flame was studied in an axisymmetric cylindrical combustion chamber, focusing on thermal radiation effects on temperature and soot concentration fields. The simulation is based on the solution of the mass, energy, momentum and chemical species conservation equations. The turbulence and its interaction with combustion are modelled by the standard k-ε model and eddy dissipation concept, respectively. The semi-empirical model of Syed is implemented to deal with soot formation and oxidation and thus ensuring the overall efficiency of the present investigation. The radiative heat transfer is surveyed, for two cases: with and without soot radiation. The numerical resolution has been achieved using the Hottel's zonal method and the standard weighted-sum-of-gray-gases model, to predict the real gas-soot mixture radiation effect. A new concept of optical exchange gap has been recently proposed and applied here after avoiding the singularities obviously encountered in the calculation of the direct exchange areas of volume zones self-irradiance. The obtained numerical results are compared to experimental data due to Brookes and Moss. Radiation exchange is found to noticeably affect temperature and soot volume fraction predictions and slightly the mixture fraction solutions. The present paper shows that taking into account turbulent combustion-radiation interactions leads to more accurate results by comparison to available experimental data.

Keywords: Turbulent combustion, Soot radiation, Zonal method, Optical exchange gap (OEG), WSGG model.

1. Introduction

Radiative heat transfer plays an important role in many thermal industrial processes such as boilers and furnaces or other gas-fired combustion systems. To acquire a better understanding of the non-premixed combustion, the inclusion of

Nomenclatures

A_i	Area of surface zone, m^2
$a_{g,n,m}$, $a_{w,n,m}$	WSGG model weighting factors
C_p	Specific heat, $J.kg^{-1}.K^{-1}$
C_s	Soot concentration, $kg.m^{-3}$
$C_\mu, C_{\varepsilon 1}, C_{\varepsilon 2}$	Constants of the standard k-ε model
$C_\alpha, C_\beta, C_\gamma, C_\sigma$	Constants of the Syed model
D	Mixture mass diffusivity, $m^2.s^{-1}$
d_p	Diameter of soot particle, m
E_w°, E_g°	Black body emissive power, $W.m^{-2}$
f_v	Soot volume fraction
	Specific enthalpy, $J.kg^{-1}$
k	Kinetic energy, $m^2.s^{-2}$
K_A, K_B, K_T, K_Z	Rate constants in Nagle and Strickland-Constable model
k_g	Specific absorption coefficient for the gas mixture, $m^{-1}.atm^{-1}$
k_s	Specific absorption coefficient for soot, $m^{-1}.atm^{-1}$
k_{CH_4}	Specific absorption coefficient for methane, $m^{-1}.atm^{-1}$
K_t	Attenuation coefficient of the medium, m^{-1}
M	Molecular mass, $g.mol^{-1}$
N_A	Avogadro number, $N_A=6.022\ 10^{23}$
N_g	Number of gray gases required for a gas mixture
N_s	Number of gray gases required for a soot
P	Pressure, atm
P_{O2}	Oxygen partial pressure, atm
P_k	Production rate of turbulent kinetic energy, $kg.m^{-1}.s^{-3}$
Pr	Prandtl number
$\vec{r}_{ij}$	Distance vector from zone i to zone j
r	Radial coordinate, m
R_i, R_f	Volumetric rate of formation or destruction of i^{th} specie and fuel, respectively.
Sc	Schmidt number
S_{rad}	Radiative source term, $W.m^{-3}$
$\overline{s_i s_j}$, $\overline{s_i g_j}$, $\overline{g_i g_j}$	Direct exchange areas, m^2
$\overrightarrow{S_i G_j}$, $\overrightarrow{G_i G_j}$	Directed flux areas, m^2
T	Temperature, K
T_α, T_γ	Activation temperatures, K
U,V	Axial and radial velocity, $m.s^{-1}$
V_k	Volume of gas zone, m^3
x	Axial coordinate, m
Y	Mass fraction

Subscripts

f	fuel
g	gas-soot mixture
i, j	species or surface zone
k	volume zone
ox	oxidant

pr	product
s	soot
t	turbulent
w	Wall

Superscripts

°	reference
~	density weighted mean
−	mean value

Greek Symbols

χ	Constant in Nagle and Strickland-Constable model
ε	Dissipation rate of kinetic energy, $m^2.s^{-3}$
ϕ_n	Soot particle density
ϕ_s	Soot mass fraction
Γ_g	Number of volume zones
Γ_s	Number of surface zones
κ	Thermal conductivity, $W.\ m^{-1}.\ K^{-1}$
μ	Laminar dynamic viscosity, $kg.m^{-1}.s^{-1}$
θ	Angle between normal to surface zone i and $\vec{r}_{ij}$
ρ	Density, $kg.\ m^{-3}$
σ_k	Prandtl number of kinetic energy
σ_ε	Prandtl number of dissipation rate
ω_{ox}	Specific soot oxidation rate per unit surface, $kg.m^{-2}.s^{-1}$.

Abbreviations

DOM	Discrete ordinate method
DEAs	Direct exchange areas, m^2
DFAs	Directed flux areas, m^2
EDC	Eddy dissipation concept
FVM	Finite volume method
NB-WSGG	Narrow-Band based weighted sum of gray gases
OEG	Optical exchange gap
PDE	Partial differential equation
RTE	Radiative transfer equation
TEAs	Total exchange areas, m^2
WSGG	Weighted sum of gray gases

radiation heat transfer into combustion modelling represents a fundamental improvement in the complex numerical modelling of turbulent non-premixed flames. Flows with combustion are almost always of a turbulent nature. That is why taking into account the turbulence through appropriate available models is indispensable. Many studies are devoted to this subject. For example, Gazzah and Sassi [1] have presented a numerical study of the turbulent non-isothermal axisymmetric jet. They employed two k-ε closure models based on Favre or Reynolds averaging. The main objective of this work is to quantify the accuracy of the two mentioned models. The authors have shown that only the Reynolds averaging approach permits to treat the anisotropy of mass flux. Tabet et al. [2] studied a co-flow axisymmetric turbulent non-premixed hydrogen flame. This study checked out the advantages of two turbulence models which are the k-ε and

the Reynolds Stress (RS) models. Results demonstrated that the predictions based on the RS model are visibly better than those obtained using the k-ε model, when close to the nozzle and the flame tip. Nevertheless, further downstream, the results are slightly in favour of k-ε model. In order to circumvent the shortcoming of the linear k-ε based turbulence model, Han and Reitz [3] used the modified Re-Normalization Group (RNG) k-ε model which is introduced successfully to simulate the spray combustion.

An extensive importance has been dedicated by many researchers to simulate the radiative heat transfer in cartesian and cylindrical geometry in many industrial situations [4, 5]. The effects of the radiative properties in the fluid flow and the heat transfer behaviour, with an unsteady natural convection and thermal radiation, inside a heat exchanger have been recently undertaken [6]. In the literature, several models have been developed to solve the radiative heat transfer equation (RTE). These methods can be classified into two-categories: the flux and hybrid methods. Among flux methods, the P-N method uses an expansion in terms of spherical harmonics [7]. This method avoids the resort to the formal solution of the integro-differential RTE. Among the hybrid methods, the discrete ordinates method (DOM), initially developed by Fiveland [8], is the most widely used one. Advances in the DOM reported in the last decade were presented by Coelho [9]. Many of these advances have aimed at the mitigation of the drawbacks of this method. The author presented new spatial and angular discretization schemes to palliate the false scattering and ray effect. Méchi et al. [10] employed the Hottel's zone method [11] based on the concept of the exchange areas associated with the weighted sum of gray gases (WSGG) model to investigate an inhomogeneous and non-gray media confined in a rectangular furnace. In this work, the most popular WSGG model parameters due to Truelove [12], Farag [13] and Smith et al. [14] have been adopted. Direct exchange areas (DEAs) are numerically carried out then adjusted to meet energy conservation constraints using two-smoothing methods, the least squares [15] and the Lawson method [16] generalized by Méchi et al. [10].

In a recent mathematical modelling analysis of the thermal radiation in a fired axisymmetric cylindrical enclosure, Farhat et al. [17] have proposed a new concept of optical exchange gap (OEG) allowing the DEAs to be successfully estimated using a rigorous integration technique based on the trapezoidal integration scheme together with the Richardson acceleration technique [18]. The authors have thoroughly discussed how to circumvent the problem of the singularities obviously encountered in the calculation of four, five and sixfold integrals to carry out the DEAs for any adjacent zones and volume zones themselves (self-irradiance). The reduced integration scheme (RIS) has been recently extended by Li et al. [19] to calculate the DEAs in a three-dimensional rectangular furnace. The former was firstly proposed by Erkku [20] for uniformly zones dividing cylindrical system, then applied by Tian and Chiu [21] for nonuniformly ones, where it was shown that with the help of the RIS, the singularities of DEAs are decomposed and weakened.

Gassoumi et al. [22] used the finite volume method (FVM), initially developed by Raithby and Chui [23], to solve the RTE for a non-gray medium containing a gas-soot mixture. The radiative properties, calculated by the narrow-band based weighted-sum-of-gray-gases model (NB-WSGG) [24] are affected by radiation resulting from hot gas, soot particles and surrounding combustor walls.

The RTE has been solved with FVM using new expressions of the coefficients appearing in the discretized angular redistribution term [25]. Several authors analysed the radiative effect on the thermal behaviour of an axisymmetric turbulent flame. Silva et al. [26] and Felipe et al. [27] simulated numerically a turbulent non-premixed flame and showed the importance of the thermal radiative interchange to obtain reliable predictions. The authors resolved the RTE, respectively using the zonal method [11] and DOM [8], both associated with the WSGG model. Bidi et al. [28] modelled the turbulence, chemistry and radiation interactions within an axisymmetric premixed flame. Radiation modelling is performed similarly to that in [27]. The obtained results of the temperature and species concentrations were found in good agreement with experimental data if the non-gray air-combustion gaseous products were considered radiatively active.

The current study is an analysis of the thermal radiation in a turbulent non-premixed methane-air flame within an axisymmetric cylindrical configuration. The RTE was solved using the zonal method based on the exchange areas, associated with the WSGG model to account for the spectral dependance of the gas-soot mixture radiative properties [12]. The combustion products derived from the turbulent non-premixed flame are composed in a major fraction of soot particulates suspended in a gaseous atmosphere containing a mixture of carbon dioxyde (CO_2), water vapour (H_2O), methane (CH_4) and other transparent gaseous species like dihydrogen (H_2) and nitrogen (N_2). The numerical results arising from the abovementioned mathematical model used in the present work, concern the medium temperature, mixture fraction and soot volume fraction distributions, along the axial and radial directions. In this paper, we set out to compare these findings to experimental data addressed by Brookes and Moss [29].

2. Mathematical Model

2.1. Governing equations

In this section, the conservation equations for the turbulent combustion flow are presented for the cylindrical coordinates system (r, x), taking advantage of axisymmetry and assuming that:

- buoyancy is absent
- gravity force are negligible
- pressure in the flow is uniform.
- in the axial direction, diffusion, heat transfer by conduction and viscous force are negligible.

For these hypotheses, conservation equations are written as [27]:

- Continuity equation

$$\frac{\partial(\bar{\rho}\tilde{U})}{\partial x}+\frac{\partial(\bar{\rho}\tilde{V})}{\partial r}+\frac{\bar{\rho}\tilde{V}}{r}=0 \tag{1}$$

- Momentum equation

$$\tilde{U}\frac{\partial(\bar{\rho}\tilde{U})}{\partial x}+\tilde{V}\frac{\partial(\bar{\rho}\tilde{U})}{\partial r}=-\frac{\partial P}{\partial x}+\vec{\nabla}\left[(\mu+\mu_t)\vec{\nabla}\tilde{U}\right]+\frac{\partial}{\partial x}\left(\mu_t\frac{\partial\tilde{U}}{\partial x}\right)+\frac{1}{r}\frac{\partial}{\partial r}\left(r\mu_t\frac{\partial\tilde{V}}{\partial x}\right) \quad (2)$$

$$\tilde{U}\frac{\partial(\bar{\rho}\tilde{V})}{\partial x}+\tilde{V}\frac{\partial(\bar{\rho}\tilde{V})}{\partial r}=-\frac{\partial P}{\partial r}+\vec{\nabla}\left[(\mu+\mu_t)\vec{\nabla}\tilde{V}\right]+\frac{\partial}{\partial x}\left(r\mu_t\frac{\partial\tilde{U}}{\partial r}\right)+\frac{1}{r}\frac{\partial}{\partial r}\left(r\mu_t\frac{\partial\tilde{V}}{\partial r}\right)-\frac{(\mu+\mu_t)\tilde{V}}{r^2} \quad (3)$$

- Species transport equation

$$\tilde{U}\frac{\partial(\bar{\rho}\tilde{Y}_i)}{\partial x}+\tilde{V}\frac{\partial(\bar{\rho}\tilde{Y}_i)}{\partial r}=\vec{\nabla}\left[\left(\bar{\rho}D+\frac{\mu_t}{Sc_t}\right)\vec{\nabla}\tilde{Y}_i\right]+\bar{R}_i \quad (4)$$

where $\bar{R}_i$ is the average volumetric rate of formation or destruction of the i-th chemical specie. The latter is obtained by summation over the volumetric rates of formation or oxidation $\bar{R}_{i,k}$ relative to the k-th balanced reaction equation where the i-th specie is present. A description of the adopted model to estimate this quantity will be presented in section 2.3.

- Energy equation

$$\tilde{U}\frac{\partial(\bar{\rho}\tilde{h})}{\partial x}+\tilde{V}\frac{\partial(\bar{\rho}\tilde{h})}{\partial r}=\vec{\nabla}\left[\left(\frac{\kappa}{C_p}+\frac{\mu_t}{Pr_t}\right)\vec{\nabla}\tilde{h}\right]+\sum_i\left[\frac{h_i^\circ}{M_i}+\int_{\tilde{T}_{ref,i}}^{\tilde{T}}C_{p,i}d\tilde{T}\right]\bar{R}_i+S_{rad} \quad (5)$$

where $\tilde{T}$ and $\tilde{h}$ are respectively the average temperature and enthalpy. h_i°, $\tilde{T}_{ref,i}$ and $C_{p,i}$ represent respectively the formation enthalpy, reference temperature and specific heat of the i-th chemical specie. S_{rad} represents the source term, Eq. (22) in energy conservation equation due to the radiative transfer.

2.2. Turbulence model

To solve the turbulent closure problem, we use the two equations k-ε model, developed by Launder and Spalding [30], where the turbulent viscosity μ_t is expressed in terms of time mean value of the kinetic energy of turbulence, $\tilde{k}$ and the volumetric turbulent kinetic energy dissipation rate, $\tilde{\varepsilon}$ as

$$\mu_t=C_\mu\bar{\rho}\frac{\tilde{k}^2}{\tilde{\varepsilon}} \quad (6)$$

The k-ε model is attractive as it only requires the solution of two equations, a relatively coarse computational mesh and can be easily implemented. The transport equations as per standard k-ε model are expressed as

- Turbulent kinetic energy

$$\tilde{U}\frac{\partial(\bar{\rho}\tilde{k})}{\partial x}+\tilde{V}\frac{\partial(\bar{\rho}\tilde{k})}{\partial r}=\vec{\nabla}\left[\left(\mu+\frac{\mu_t}{\sigma_k}\right)\vec{\nabla}\tilde{k}\right]+P_k-\bar{\rho}\tilde{\varepsilon} \quad (7)$$

- Turbulent kinetic energy dissipation rate

$$\tilde{U}\frac{\partial(\bar{\rho}\tilde{\varepsilon})}{\partial x}+\tilde{V}\frac{\partial(\bar{\rho}\tilde{\varepsilon})}{\partial r}=\vec{\nabla}\left[\left(\mu+\frac{\mu_t}{\sigma_\varepsilon}\right)\vec{\nabla}\tilde{\varepsilon}\right]+\frac{\tilde{\varepsilon}}{\tilde{k}}\left(C_{\varepsilon_1}P_k-C_{\varepsilon_2}\bar{\rho}\tilde{\varepsilon}\right) \quad (8)$$

where P_k is given by

$$P_k=\mu_t\left[2\left(\frac{\partial\tilde{U}}{\partial x}\right)^2+\left(\frac{\partial\tilde{U}}{\partial r}+\frac{\partial\tilde{V}}{\partial x}\right)^2+2\left(\frac{\partial\tilde{V}}{\partial r}\right)^2+2\left(\frac{\tilde{V}}{r}\right)^2\right] \quad (9)$$

The constants C_μ, C_{ε_1}, C_{ε_2}, σ_k and σ_ε that intervene in this model are available in Table 1.

Table 1. Constants of the standard k-ε model [30].

C_μ	C_{ε_1}	C_{ε_2}	σ_k	σ_ε
0.09	1.44	1.92	1.0	1.3

2.3. Combustion model

A single step balanced chemical equation of the combustion of a lean methane (CH_4) and air mixture is given as [31]

$$CH_4+2\ (O_2+3.76\ N_2)\rightarrow CO_2+2\ H_2O+7.52\ N_2 \quad (10)$$

The main challenge in modelling turbulent combustion phenomena resides in the closure of the mean volumetric rate of reaction $\bar{R}_i$, Eqs. (4) and (5). Here comes the turbulent combustion modelling, where the eddy dissipation concept [32] is adopted. The reaction rate $\bar{R}_f$ for the fuel is defined as

$$\bar{R}_f=-a\,\bar{\rho}\,\frac{\tilde{\varepsilon}}{\tilde{k}}\,min\left(\tilde{Y}_f\frac{\tilde{Y}_{ox}}{s},\ b\frac{\tilde{Y}_{pr}}{1+s}\right) \quad (11)$$

where (a, b)=(4.0, 0.5) are the model constants and s represents the stoichiometric oxygen required to burn one kilogram of fuel.

2.4. Soot model

To predict soot formation, the Syed model is used [33]. Two-additional transport equations are solved. The first equation accounts for the transport of soot particle density, and the second one describes the transport of the soot mass fraction. Nucleation, surface growth and oxidation effects are taken into account in the formulation. The particles are assumed to be spherical and having a size distribution which is simply represented by an average diameter d_p through the following expression [34]

$$d_p = \sqrt[3]{\frac{6f_v}{\rho \pi N_A \phi_n}} \tag{12}$$

The transport equation for the particle density ϕ_n and the soot mass fraction, ϕ_s are respectively given by [33]

$$\tilde{U}\frac{\partial(\bar{\rho}\tilde{\phi}_n)}{\partial x} + \tilde{V}\frac{\partial(\bar{\rho}\tilde{\phi}_n)}{\partial r} = \vec{\nabla}(\bar{\rho}D\vec{\nabla}\tilde{\phi}_n) + \tilde{S}_{\phi_n} \tag{13-a}$$

$$\tilde{U}\frac{\partial(\bar{\rho}\tilde{\phi}_s)}{\partial x} + \tilde{V}\frac{\partial(\bar{\rho}\tilde{\phi}_s)}{\partial r} = \vec{\nabla}(\bar{\rho}D\vec{\nabla}\tilde{\phi}_s) + \tilde{S}_{\phi_s} \tag{13-b}$$

The source terms of Eqs. 13(a) and (b) can be expressed as a sum of contributions from nucleation, coagulation, particle growth and oxidation

$$\tilde{S}_{\phi_n} = \tilde{S}_{\phi_{n,nuc}} + \tilde{S}_{\phi_{n,coag}} \tag{14-a}$$

$$\tilde{S}_{\phi_s} = \tilde{S}_{\phi_{s,nuc}} + \tilde{S}_{\phi_{s,growth}} + \tilde{S}_{\phi_{s,ox}} \tag{14-b}$$

The different terms in the right hand sides of Eqs. 14(a) and (b), except the term of oxidation, are given by Syed et al. [33]

$$\tilde{S}_{\phi_{n,nuc}} = C_\alpha \bar{\rho}^2 T^{\frac{1}{2}} X_f e^{-\frac{T_\alpha}{T}} \tag{15-a}$$

$$\tilde{S}_{\phi_{n,coag}} = C_\beta \bar{\rho}^2 T^{\frac{1}{2}} \tilde{\phi}_n^{\,2} \tag{15-b}$$

$$\tilde{S}_{\phi_{s,nuc}} = C_\sigma C_\alpha \bar{\rho}^2 T^{\frac{1}{2}} X_f e^{-\frac{T_\alpha}{T}} \tag{15-c}$$

$$\tilde{S}_{\phi_{s,growth}} = \bar{\rho}^2 C_\gamma N_o^{\frac{1}{3}} T^{\frac{1}{2}} X_f \tilde{\phi}_n^{\frac{1}{3}} \tilde{\phi}_s^{\frac{2}{3}} e^{-\frac{T_\gamma}{T}} \tag{15-d}$$

In the above equations, X_f is the mole fraction of the fuel (CH_4), T_α and T_γ are activation temperatures for nucleation and growth, respectively. The constants of Syed model are provided in Table 2 for methane.

Table 2. Constants of the Syed model [33].

Fuel	Methane
$C_\alpha \left(\mathbf{m^3.kg^{-2}.K^{-\frac{1}{2}}.s^{-1}}\right)$	6.54×10^4
$C_\beta \left(\mathbf{m^3.K^{-\frac{1}{2}}.s^{-1}}\right)$	1.3×10^7
$C_\gamma \left(\mathbf{m^3.kg^{-\frac{2}{3}}.K^{-\frac{1}{2}}.s^{-1}}\right)$	0.1
C_σ (kg)	144
T_α (K)	46100
T_γ (K)	12600

The volumetric oxidation rate of soot is given by [33]

$$\tilde{S}_{\phi_{s,ox}} = \bar{\rho}\left(\frac{36\pi}{\rho_s^2}\right)^{\frac{1}{3}} N_o^{\frac{1}{2}} \tilde{\phi}_n^{\frac{1}{2}} \tilde{\phi}_s^{\frac{2}{3}} \omega_{ox} \tag{16}$$

where ρ_s is the soot particulate density (=1800 kg/m^3) [34]. The specific oxidation rate per unit surface, ω_{ox}, is calculated using the model of Nagle and Strickland-Constable [35]

$$\omega_{ox} = 120\left[\frac{K_A P_{O_2}\chi}{1+K_Z P_{O_2}} + K_B P_{O_2}(1-\chi)\right] \tag{17}$$

where

$$K_A = 20e^{-\frac{25098}{T}} \tag{18-a}$$

$$K_B = 4.46\ 10^{-3} e^{-\frac{7650}{T}} \tag{18-b}$$

$$K_Z = 21.3\ e^{\frac{2053}{T}} \tag{18-c}$$

$$K_T = 1.511\ 10^5 e^{-\frac{48817}{T}} \tag{18-d}$$

$$\chi = \left(1+\frac{K_T}{K_B P_{O_2}}\right) \tag{18-e}$$

2.5. Radiation model

The zonal method of analysis, originally developed by Hottel and Sarofim [11], is based on the concept of exchange areas. These interchange areas are of three types: direct exchange areas (DEAs), total exchange areas (TEAs) and directed flux areas (DFAs). The physical system under consideration is divided into given surface and volume zones. The spatial meshing is selected so that nodes occupied the centre of a surface area or volume zone. In homogeneous and inhomogeneous non-gray semi-transparent media, the DEAs are defined by [36]

$$\overline{s_i s_j} = \int_{A_i}\int_{A_j} \frac{\cos\theta_i \cos\theta_j\, exp\left(-\int_0^{r_{ij}} K_t(s')ds'\right)}{\pi r_{ij}^2} dA_i dA_j = \overline{s_j s_i} \tag{19-a}$$

$$\overline{s_i g_j} = \int_{A_i}\int_{V_j} \frac{K_{t,j}\cos\theta_i\, exp\left(-\int_0^{r_{ij}} K_t(s')ds'\right)}{\pi r_{ij}^2} dA_i dV_j = \overline{g_j s_i} \tag{19-b}$$

$$\overline{g_i g_j} = \int_{V_i}\int_{V_j} \frac{K_{t,i}K_{t,j} exp\left(-\int_0^{r_{ij}} K_t(s')ds'\right)}{\pi r_{ij}^2} dV_i dV_j = \overline{g_j g_i} \tag{19-c}$$

The DEAs data obey the conservation constraints commonly known as the summation rules which are written for a surface zone j [21]

$$\sum_{i=1}^{\Gamma_s} \overline{s_j s_i} + \sum_{k=1}^{\Gamma_g} \overline{s_j g_k} = A_j \qquad j = 1, \ldots \Gamma_s \tag{20}$$

and for a volume zone k

$$\sum_{i=1}^{\Gamma_s} \overline{g_k s_i} + \sum_{j=1}^{\Gamma_g} \overline{g_k g_j} = 4K_t V_k \qquad k = 1, \ldots \Gamma_g \tag{21}$$

Calculation of DEAs is performed with desired accuracy using Romberg's integration method which associates the trapezoidal rule and Richardson extrapolation formula [18]. A new concept of optical exchange gap (OEG) recently proposed by Farhat et al. [17] is applied to overcome the drawback of singular DEAs of self-irradiance of gas volume zones. The OEG represents the optical path width around singularity where radiation energy exchange between volume elements is imperceptible. The OEG widths are deduced using a correlation depending on the radial position and optical thickness. This concept has proved to be more efficient, simple and accurate than a proper center-to-center technique [37, 38]. DEAs are adjusted to meet Eqs. (20) and (21) using the least squares method [15]. The TEAs are derived from adjusted DEAs using some explicit matrix relations [39]. The former are generally used to calculate the net radiative heat flux in gray participating media. For a non-gray medium, the net radiative heat flux per unit volume in a given gas zone, is expressed in terms of the so-called DFAs as proposed by Rhine and Tucker [40]

$$S_{rad}=-\frac{1}{V_i}\left[4\sum_{n=1}^{N_g}\sum_{m=1}^{N_s}\left(a_{g,n,m}K_{t,n,m}\right)_i V_i E^o_{g,i}-\sum_{j=1}^{\Gamma_g}\overrightarrow{G_jG_i}E^o_{g,j}-\sum_{j=1}^{\Gamma_s}\overrightarrow{S_jG_i}E^o_{w,j}\right] \tag{22}$$

The left hand side of Eq. (22) is equal in magnitude and opposite to the radiative source term that appears in the energy equation (Eq. (5)). $\overrightarrow{G_jG_i}$ and $\overrightarrow{S_jG_i}$ are respectively the DFAs corresponding to the gas-to-gas and surface-to-gas radiative exchange given by

$$\overrightarrow{G_jG_i}=\sum_{n=1}^{N_g}\sum_{m=1}^{N_s}a_{g,n,m}\left(T_{g,j}\right)\left(\overline{G_iG_j}\right)_{K_{t,n,m}} \tag{23-a}$$

$$\overrightarrow{S_jG_i}=\sum_{n=1}^{N_g}\sum_{m=1}^{N_s}a_{w,n,m}\left(T_j\right)\left(\overline{G_iS_j}\right)_{K_{t,n,m}} \tag{23-b}$$

where N_g and N_s are the numbers of gray gases simulating the non-gray behaviour of the gas mixture and soot particles, respectively [12]. The DFAs are calculated simply by summation of the TEAs overall the gray gases weighted by the coefficients $a_{g,n,m}$ and $a_{w,n,m}$ which are polynomials on the local temperatures of the gas and surface zones, respectively. These coefficients are obtained by fitting the total emissivity of absorption and/or emission contributors (mainly CO_2, H_2O and soot in gas fired combustion systems) to the total emissivity calculated by the exponential wide band model (EWB). Similar expressions of the DFAs can be written for the surface-to-surface and gas-to-surface radiative exchange [41]. $K_{t,n,m}$ is the absorption coefficient for the (n, m) gray gas ($K_{t,n,m}=k_{g,n}P+k_{s,m}C_s+k_{CH_4,n}P_{CH_4}$). For a gas mixture, P is the sum of the partial pressures of the radiatively absorbing species (mainly CO_2 and H_2O). The weighting factors $\left(a_{g,n,m},\ a_{w,n,m}\right)$ and the specific gray gas absorption coefficients $\left(k_{g,n},k_{s,n},k_{CH_4,n}\right)$ are the WSGG model's parameters. In the present numerical simulation, we set out to choose the parameters due to Truelove [12] for a water vapour and carbon dioxide pressure ratio equal to 2.

3. Method of Solution

The finite volume method (FVM) is used to solve the mass, energy, momentum and chemical species conservation equations by means of a Fortran code. The partial differential equations (PDEs) are discretized by using a staggered-mesh. Velocity components are defined at the cell faces whereas scalar variables are defined at the cell center. The control volume is as indicated in Fig. 1.

The resulting system of algebraic equations was solved by the Tri-Diagonal-Matrix-Algorithm (TDMA) and the pressure-velocity coupling was made by the SIMPLE method [42]. The convergence criterion is satisfied when the maximum value of normalized residuals of any equation is less than 10^{-3}. A sensitive grid mesh study has already been done. Numerical results for radial and axial temperature distributions are quite similar when increasing the number of surface and volume zones. Therefore, a numerical mesh of (r, x) = 60×45 grid nodes is adopted. However, to assess radiation exchanges, DEAs are evaluated using a less refined grid mesh (15×15) in order to control the computation time required for all the gray gases used in this study to represent the real gas-soot mixture in the context of the WSGG model [12].

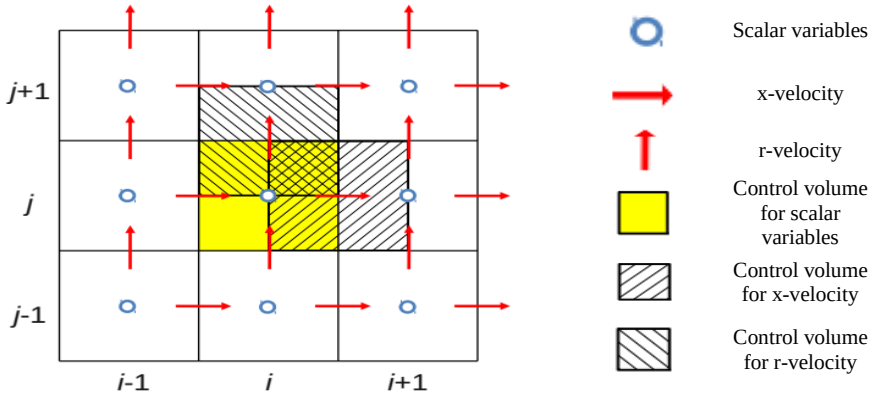

Fig. 1. Staggered mesh.

4. Results and Discussions

The mathematical procedure based on the different models outlined previously is applied to a methane-air turbulent diffusion flame, where this case study has already been experimentally conducted by Brookes and Moss [29]. At an ambient temperature, methane is introduced through a nozzle with a diameter of 4.07 mm, at an average velocity of 20.3 m/s. The air is supplied through an annulus surrounding the nozzle at an average velocity of 0.55 m/s. The physical system boundaries, confining the open flame, are supposed to be black. Table 3 lists the experimental conditions of this flame. All the results of the mixture fraction, temperature, and soot volume fraction distributions obtained in the present study are compared to experimental data [29]. In table 3, Reynolds number is obtained by dividing the gas (methane) velocity and the nozzle diameter product, by the kinetic viscosity of the methane. Due to the symmetry of physical system, a geometrical simplified axisymmetric computational model is used (Fig. 2). Table 4 summarizes the boundary conditions applied to the computational domain.

Table 3. Operating conditions for the studied flame [29].

Fuel	Methane
Fuel temperature [K]	290
Nozzle diameter [mm]	4.07
Fuel velocity [m/s]	20.3
Reynolds Number (at methane exit)	5000
Air velocity [m/s]	0.55
Stoichiometric mixture	0.055
Pressure [atm]	1

Table 4. Boundary conditions.

Region	Boundary Condition
Fuel Inlet	Inlet Boundary condition with 20.3 m/s of fuel velocity and 5% turbulent intensity
Coflow	Inlet Boundary condition with 20.3 m/s of fuel velocity and 5% turbulent intensity
Outer Side	Wall
Outlet	Pressure boundary condition
Symmetry	Symmetry Boundary condition

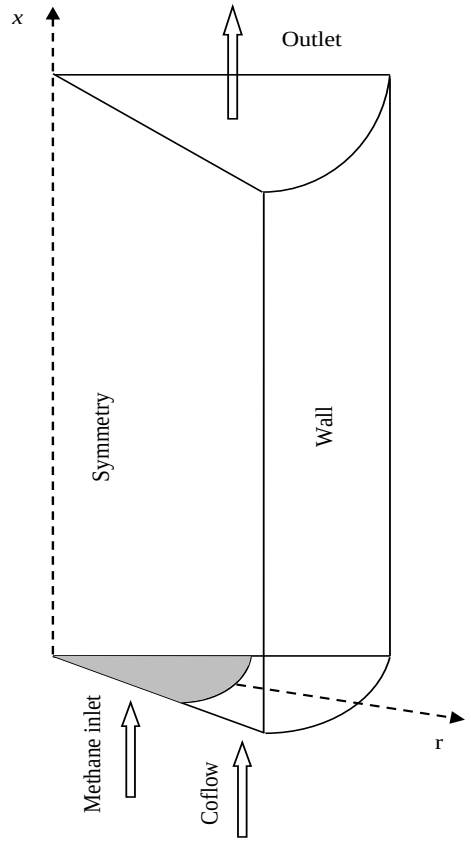

Fig. 2. Axisymmetric computational domain.

4.1. Mixture fraction

Figure 3 is a comparison between the centreline mixture fraction of methane flame obtained numerically and those taken from the experimental data for three cases (with radiation, without radiation and without soot radiation), in order to assess the effect of radiation interchange in the considered domain. The mean mixture fraction is decreasing rapidly when the co-flowing air is led and mixed with the fuel. The centreline mixture fraction is predicted using a combination of the standard k-ε turbulence model and eddy dissipation concept (EDC). A good fitting is obtained between simulated and experimental data due to Brookes and Moss [29], except at a distance ranging between 50 and 150 mm above the nozzle where the mixture fraction is under-predicted. This might be due to the lack of rigorousness in the representation of combustion chemistry by the EDC.

Figure 3 depicts that the centreline mixture fraction profile is weakly influenced by radiation whether the radiation of soot is neglected or not. This can be explained by the fact that thermal radiation exchange has a very little effect on the chemical reactions in the chamber centreline. This is because the chemical reaction rate $\bar{R}_i$ (Eqs. (4) and (5)) is controlled by turbulent mixing and therefore is less sensitive to temperature gradient (Eq. (11)).

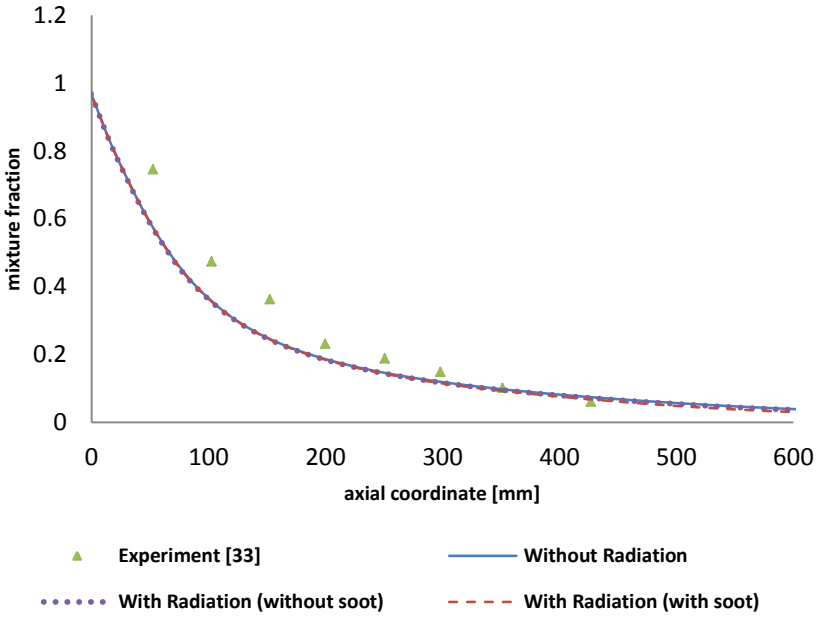

Fig. 3. Centreline axial profile of the mixture fraction with and without radiation.

Predicted radial mixture fraction profiles at flame heights of 150, 200, 250, 300, 350 and 425 mm are compared to experimental data in Fig. 4. A better agreement is achieved if the radiative heat transfer is considered. In the fuel poor zone that is beyond the flame (i.e., x=300–425 mm), radiation has a greater effect on the mixture fraction predictions than elsewhere (i.e., x=150–250 mm) because

the major species present are the most radiatively active (H_2O, CO_2). The results found in this section confirm those recently shown by Centeno et al. [43]. The authors demonstrated that the influence of soot radiation on the concentrations of the main chemical species proved negligible.

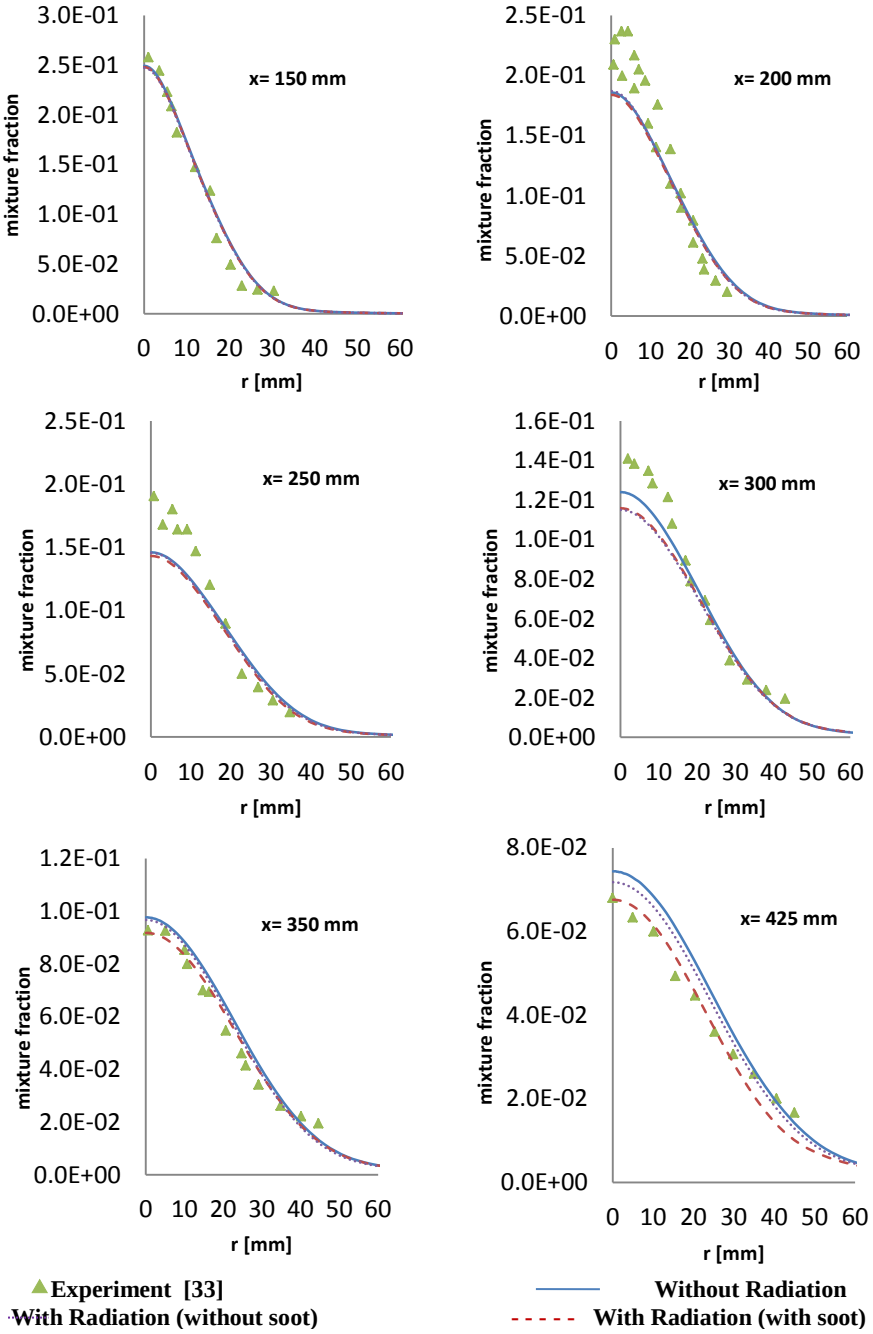

Fig. 4. Radial profiles of the mixture fraction for different axial locations.

4.2. Temperature field

Three scenarios have been considered to study the effect of the gas radiation on the temperature distribution within the domain under discussion. In the first scenario, radiation is completely ignored, in the second scenario, radiation from gas only is accounted for, while in the last one, radiation from gases and soot is incorporated in the calculation. Figure 5 compares the predicted axial temperature for three cases and the experimental measurements. It is shown that the temperature profiles obtained by the numerical model including radiation for two scenarios (with radiation from gases and soot and without soot radiation) have almost the same degree of accuracy than the one without radiation up to an axial distance of 100 mm from the nozzle outlet. This is foreseeable as the most radiating species (i.e., H_2O, CO_2 and soot) are not massively produced yet. Beyond this distance, the axial temperature profiles calculated with radiation using the zonal method better fit the experimental data due to Brookes and Moss [29]. We also note that the influence of soot radiation on the temperature is seen only in the region of higher temperatures (x > 350 mm).

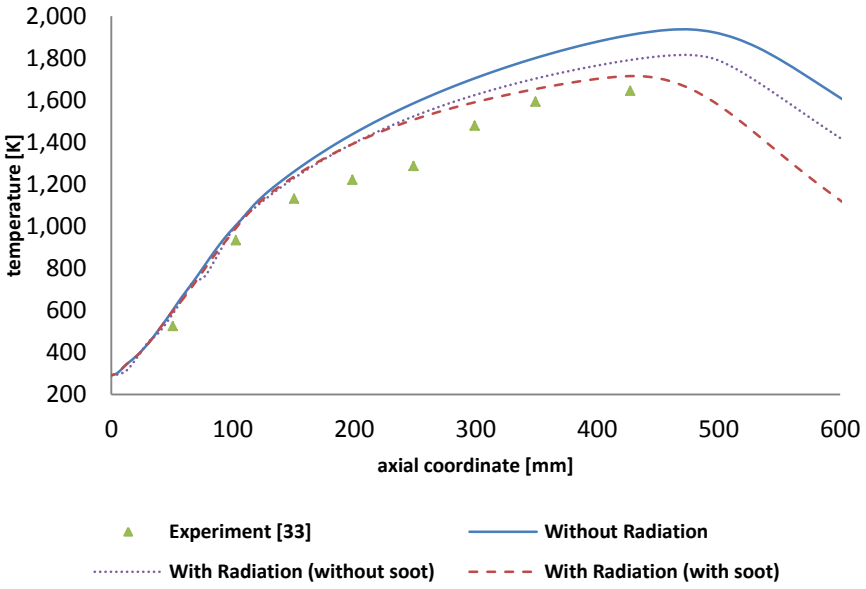

Fig. 5. Centreline axial profile of the temperature with and without radiation.

The model failed to attempt experimental data in the region between 150 and 250 mm closer to the nozzle. This discrepancy is mainly due to the inefficiency of the eddy dissipation concept, which neglects the combustion kinetic as the combustion reaction is represented by a single step reaction. Figure 6 presents the temperature distributions along the radial direction at six different axial locations for three cases (with radiation from gas, with radiation from gas and soot and without radiation).

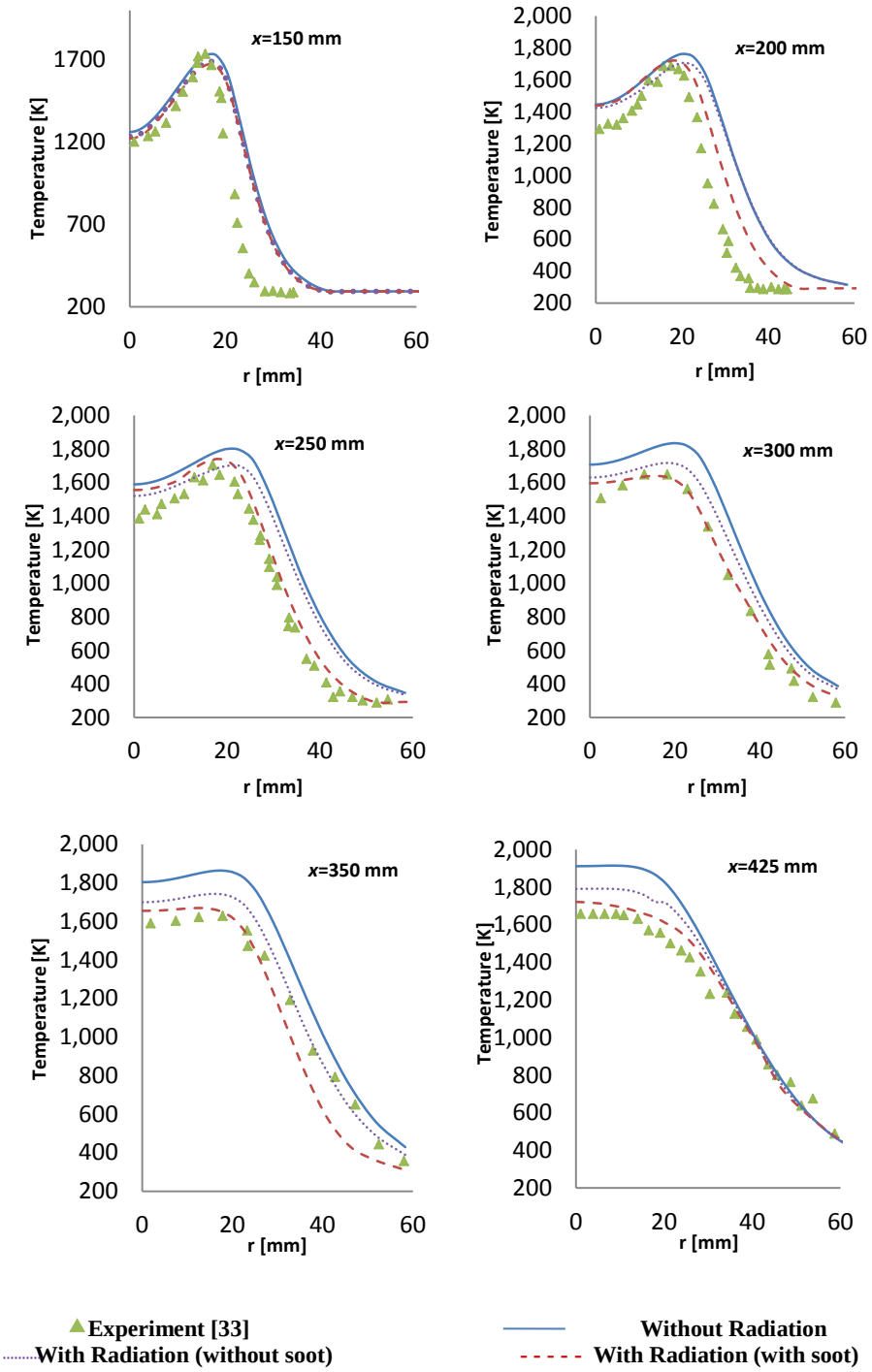

Fig. 6. Radial profiles of the temperature for different axial positions.

The results show that the radial temperature distributions at the axial locations 150, 200, 250, 300, 350 and 425 mm have similar trends to those of the experimental data and that the inclusion of thermal radiation results in a reduction in the temperature values. The maximum temperature estimated numerically decreases for both scenarios with radiation from gas only and with radiation from gas and soot. The discrepancy from the measured temperatures of the solutions calculated with and without radiation is increasingly important as we move far from the jet exit. Observing Figs. 5 and 6, the temperature profiles agree satisfactorily with available experimental data, mainly in the high temperature zones if soot and gas radiation is considered. Besides, the maximum average temperature discrepancy does not exceed 8.8% as shown in Table 5.

Table 5. Average percentage relative temperature difference between experimental and numerical results for both radiative scenarios.

Axial position x (mm)	Without Radiation	With Radiation (without soot)	With Radiation (with soot)
300	13.5	8.3	6.0
350	13.6	7.1	4.1
425	16.1	8.8	4.2

4.3. Soot volume fraction

Figure 7 is a comparison of the axial and radial predictions of soot volume fractions ($f_v=\rho\phi_s/\rho_s$) to the experimental data from Brookes and Moss [29]. It is worth noting that the centreline soot volume fraction profile is very well described by the semi-empirical model of Syed [33] and that the radiation model is satisfactorily accurate in predicting the soot volume fraction within the flow field for two cases with and without soot radiation. Neglecting the effects of soot radiation, results in an over prediction of the soot volume fraction. A decrease of the peak value is observed when radiation from soot is accounted for. Without radiation, the predicted maximum soot volume fraction is nearly 3 times higher than with the full radiation model. The results clearly prove the strong effect of radiation on soot volume fraction predictions.

Actually, with radiation, the medium temperature tends to be uniform resulting in a strong drop of the soot source terms. This is foreseeable as these terms due to nucleation, growth and oxidation are decreasing exponentially (Eqs. 15 (c-d) and 16). This illustrates that the soot model used here described thoroughly the temperature dependence of the soot volume fraction. The prediction of soot volume fraction in the region close to the nozzle is more satisfactory (i.e., x=300 and 350 mm). However, one can state that the Hottel's zonal radiation model has widely improved the prediction of the soot volume fraction profiles in both radial and axial directions.

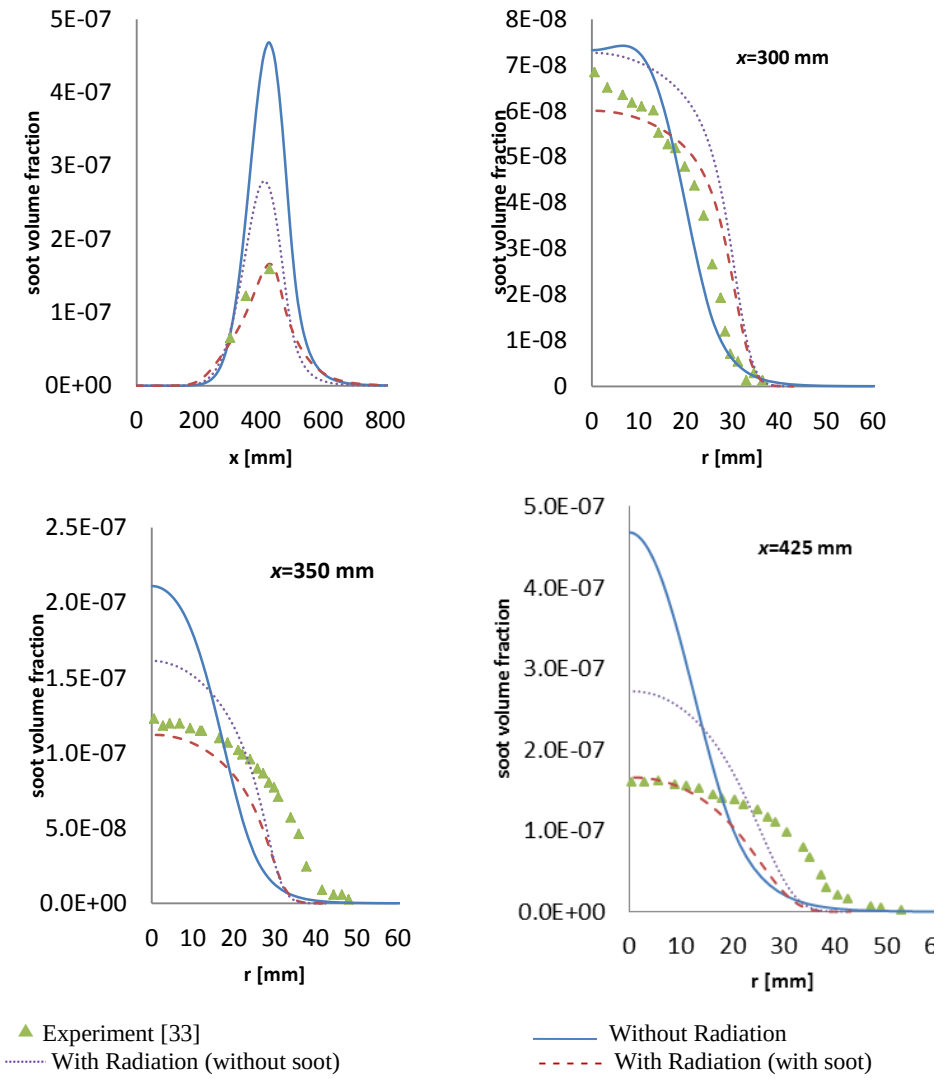

Fig. 7. Axial and radial profiles (for different axial locations) of the soot volume fraction.

5. Conclusion

The main goal of this study is to illustrate the effect of the thermal radiation interchange in a turbulent non-premixed flame for an axisymmetric cylindrical configuration. In particular, the focus has been accentuated on the interaction of radiation with the turbulent combustion assessed by means of the eddy dissipation concept (EDC) and k-ε turbulence model. In order to predict the spatial distribution of soot volume fraction, the semi-empirical soot model of Syed has been incorporated. This set of coupled mathematical models has been used to simulate a turbulent non-premixed flame of methane-air. Two-scenarios have been considered: in the first scenario, radiation is completely neglected, but in the

second one, radiation of the hot non-gray species is considered for two cases with and without soot radiation. Radiative exchange is calculated using the zonal method associated with the weighted sum of gray gases (WSGG) model, based on the Truelove's parameters. For the second scenario, results proved to be more satisfactory than for the first one as compared to measurements conducted by Brookes and Moss.

The main findings from this paper can be summarized as:

- The temperature and soot volume fraction profiles are clearly affected when thermal radiation is included while its role is found to be of minor importance in the spatial mixture fraction distributions for the adopted chemical reaction model.
- When radiation from gases and soot is considered, we notice a reduction in the maximum values of the medium temperature by about 150 K and the soot volume fraction by a factor of 3.
- Soot radiation contributes significantly in radiation exchanges and thus, should be modelled rigorously.
- The Syed model enhances the efficiency of the global modelling especially when brought together with a reliable radiation model.

Some perspectives for future work will focus on the representation of the chemical kinetics mechanism by several reactions, and the consideration of the effect of the radiatively active NO_x specie.

References

1. Gazzah, M.H.; and Sassi, M. (2001). Etude numérique des jets turbulents non isothermes avec deux schémas de fermeture k-ε. *Comptes Rendues de l'Académie des Sciences, Paris, série IIb Mécanique*, 329(6), 417-423.
2. Tabet, F.; Sarh, B.; and Mennou, A. (2006). A comparative study of turbulence modeling in hydrogen-air non-premixed turbulent flames. *Combustion Science and Technology*, 178(10-11), 1887-1906.
3. Han, Z.; and Reitz, R.D. (1995). Turbulence Modeling of internal combustion engines using RNG k-ε models. *Combustion Science and Technology*, 106(4-6), 267-295.
4. Ben Nejma, F.; and Slimi, K. (2010). Combined natural convection and radiation in humid air bounded by isothermal vertical walls. *High Temperatures-High Pressures*, 39(3), 209–226.
5. Sakly, A.; Mazgar, A.; Slimi, K.; and Ben Nejma, F. (2015). Thermal radiation contribution on humidification process in a cylindrical annular duct. *High Temperatures-High Pressures*, 44(3), 163–186.
6. Jbara, A.; Slimi, K.; Nasr, A.; and Mhimid, A. (2013). Radiative properties effects on unsteady natural convection inside a saturated porous medium. Application for porous heat exchangers. *Energy*, 61, 224-233.
7. Markis, J.G.; Papapavlou, C.; and Kakaras, E. (2000). A parametric study of radiative heat transfer in pulverised coal furnaces. *International Journal of Heat and Mass Transfer*, 43(16), 2961-2971.

8. Fiveland, W.A. (1988). Three-dimensional radiative heat-transfer solutions by the discrete-ordinates method. *Journal of Thermophysics and Heat Transfer*, 2(4), 309-316.
9. Coelho, P.G. (2014). Advances in the discrete ordinates and finite volume methods for the solution of radiative heat transfer problems in participating media. *Journal of Quantitative Spectroscopy and Radiative Transfer*, 178, 121-146.
10. Méchi, R.; Farhat, H.; Guedri, K.; Halouani, K.; and Said, R. (2010). Extension of the zonal method to inhomogeneous non-grey semi-transparent medium. *Energy*, 35(1), 1-15.
11. Hottel, H.C.; and Sarofim, A.F. (1995). *Radiative Transfer*. McGraw-Hill.
12. Truelove, J.S. (1976). A mixed grey gas model for flame radiation. *Report AERE-R-8494*, United Kingdom atomic energy authority harwell.
13. Farag, I.H. (1982). Non luminous gas radiation-approximate emissivity models. *Proc 7th International Heat Transfer Conference*. München, Germany, 487-492.
14. Smith, T.F.; Shen, Z.F.; and Friedman, J.N. (1982). Evaluation of coefficients for the weighted sum of grey gases model. *ASME Journal of Heat Transfer*, 104(4), 602-608.
15. Larsen, M.F.; and Howell, J.R. (1986). Least-squares smoothing of direct-exchange areas in zonal analysis. *ASME Journal of Heat Transfer*, 108(1), 239-242.
16. Lawson, D.A. (1995). An improved method for smoothing approximate exchange areas. *International Journal of Heat Mass Transfer*, 38(16), 3109-3110.
17. Farhat, H.; Méchi, R.; and Saïd, R. (2016). New optical exchange gap concept to calculate direct exchange areas in cylindrical industrial furnaces. *Applied Mathematical Modelling*, 40(5-6), 4044-4056.
18. Dutka, J. (1984). Richardson extrapolation and Romberg integration. *Historia Mathematica*, 11(1), 3-21.
19. Li, G.J.; Li, B.W.; and Sun, Y.S. (2015). Extension of the reduced integration scheme to calculate the direct exchange areas in 3D rectangular enclosures with non scattering media. *Mathematical Problems in Engineering*, 1-11.
20. Erkku, H. (1959). *Radiant heat-exchange in gas-filled slabs and cylinders*. Ph.D. Thesis. Massachustts Institute of Technology, Cambridge Mass, USA.
21. Tian, W.; and Chiu, W.K.S. (2003). Calculation of direct exchange areas for nonuniform zones using a reduced integration scheme. *Journal of Heat Transfer*, 125(5), 839-844.
22. Gassoumi, T.; Guedri, K.; and Said, R. (2010). Numerical study of the swirl effect on a coaxial jet combustor flame including radiative heat transfer. *Numerical Heat Transfer, Part A: Application: An International Journal of Computation and Methodology*, 56(11), 897-913.
23. Raithby, G.D.; and Chui, E.H. (1990). A finite-volume method for predicting a radiant heat transfer in enclosures with participating media. *ASME Journal of Heat Transfer*, 112(2), 415-423.

24. Kim, O.J.; and Song, T.H. (2000). Data base of WSGGM-Based spectral model for radiation properties of combustion products. *Journal of Quantitative Spectroscopy and Radiative Transfer*, 64(4), 379-394.
25. Salah, M.B.; Askri, F.; Slimi, K.; and Ben Nasrallah, S. (2004). A numerical resolution of the radiative transfer equation in cylindrical enclosure by the finite volume method. *International Journal of Heat and Mass Transfer*, 47(10-11), 2501-2509.
26. Silva, C.V.; França, F.H.R.; and Vielmo, H.A. (2007). Analysis of the turbulent non premixed combustion of natural gas in a cylindrical chamber with and without thermal radiation. *Combustion Science and Technology*, 179(8), 1605-1630.
27. Felipe, R.C.; Cristiano, V.S.; and Francis, H.R.F. (2014). The influence of gas radiation on the thermal behavior of a 2D axisymmetric turbulent non-premixed methane-air flame. *Energy Conversion and Management*, 79, 405-414.
28. Bidi, M.; Housseini, R.; and Nobari, M.R.H. (2008). Numerical analysis of methane-air combustion considering radiation effect. *Energy Conversion and Mangement*, 49(12), 3634-3647.
29. Brookes, S.J.; and Moss, J.B. (1999). Measurement of soot production and thermal radiation from confined turbulent jet diffusion flames of methane. *Combustion and Flame*, 116(1-2), 49-61.
30. Launder, B.E.; and Spalding, D.B. (1974). The numerical computation of turbulent flows. *Computer Methods in Applied Mechanics and Engineering*, 3(2), 269-289.
31. De Lange, H.C.; and De Goey, L.P.H. (1993). Two-dimensional methane/air flame. *Combustion Science and Technology*, 92(4-6), 423-427.
32. Magnussen, B.F.; and Hjertager, B.H. (1977). On mathematical modelling of turbulent combustion with special emphasis on soot formation and combustion. *Proceedings of the 16th Symposium International on Combustion*, the combustion inst., Pittsburgh, PA, 719-729.
33. Syed, K.J.; Stewart, C.D.; and Moss, J.B. (1990). Modelling soot formation and thermal radiation in buoyant turbulent diffusion flames. *Proceedings of the 23rd Symposium Internationl on Combustion*, the combustion inst., Pittsburgh, PA, 1533-1541.
34. Roditcheva, O.V.; and Bai, X.S. (2001). Pressure effect on soot formation in turbulent diffusion flames. *Proceedings of the 6th International Congress on Toxic combustion*, Munich, Germany, 811-821.
35. Nagle, J.; and Strickland-Constable, R.F. (1962). Oxidation of carbon between 1000 and 2000°C. *Proceedings of the 5th Carbon Conference*, Pergamon, London, 154-164.
36. Yuen, W.W. (2006). The multiple absorption coefficient zonal method (MACZM), an efficient computational approach for the analysis of radiative heat transfer in multidimensional inhomogeneous nongray media. *Numerical Heat Transfer Part B*, 49, 89-103.
37. Ebrahimi, H.; Zamaniyan, J.S.S.; Zadeh, M.; and Khalili, A.A. (2013). Zonal modeling of radiative heat transfer in industrial furnaces using simplified

model for exchange area calculation. *Applied Mathematical Modelling*, 37(16-17), 8004-8015.

38. Zhou, W.; and Qiu, T. (2015). Zone modeling of radiative heat transfer in industrial furnaces using adjusted Monte-Carlo integral method for direct exchange area calculation. *Applied Thermal Engineering*, 81, 161-167.
39. Noble, J. (1975). The zone method: explicit matrix relations for total exchange areas. *International Journal of Heat and Mass Transfer*, 18(2), 261-269.
40. Rhine, J.M.; and Tucker, R.J. (1991). *Modelling of gas-fired furnaces and boilers and other industrial heating processes*. British Gas in Association With McGraw-Hill Book Co. London.
41. Khan, Y.U.; Lawson, D.A.; and Tucker, R.J. (1997). Banded radiative heat transfer analysis. *Communications in Numerical Methods in Engineering*, 13(10), 803-813.
42. Patankar, S.V. (1980). *Numerical heat transfer and fluid flow*. Hemisphere Publishing Corporation, McGraw-Hill, New York.
43. Centeno, F.R.; Brittes, R.; França, F.H.R.; and da Silva, C.V. (2016). Application of the WSGG model for the calculation of gas-soot radiation in a turbulent non-premixed methane-air flame inside a cylindrical combustion chamber. *International Journal of Heat and Mass Transfer*, 93, 742-753.